Reprinted from *J. Mol. Biol.* (1994) **239**, 581–587

Five Viral Peptide–HLA-A2 Co-crystals

Simultaneous Space Group Determination and X-ray Data Collection

David N. Garboczi, Dean R. Madden and Don C. Wiley

J. Mol. Biol. (1994) **239**, 581–587

Five Viral Peptide–HLA-A2 Co-crystals

Simultaneous Space Group Determination and X-ray Data Collection

David N. Garboczi[1], Dean R. Madden[1]† and Don C. Wiley[1,2]

[1]*Department of Biochemistry and Molecular Biology and*
[2]*Howard Hughes Medical Institute,*
Harvard University
7 Divinity Avenue, Cambridge, MA 02138, U.S.A.

We prepared and crystallized five complexes of the human histocompatibility molecule HLA-A2 with peptides derived from human immunodeficiency virus type 1, human T lymphotropic virus type 1, influenza A virus and hepatitis B virus proteins. Each HLA-A2 complex was refolded *in vitro* from insoluble proteins produced in bacteria; to crystallize, two of the complexes required seeding with microcrystals of another complex. Maintained at −160°C, single co-crystals of each of the five peptide–HLA-A2 complexes yielded complete X-ray diffraction data sets to a resolution of approximately 2·5 Å. After a sufficient number of diffraction peaks were acquired during data collection, the direct analysis of integrated intensities established the point group of the co-crystal, thus allowing an efficient data collection strategy to be designed. The subsequent examination of systematic absences revealed that the five peptide–HLA-A2 co-crystals formed in space groups $P1$, $P2_1$, or $P2_12_12_1$. Molecular replacement structure solutions yielded unambiguous protein electron density maps, thus confirming the space group determinations. The system of obtaining HLA-A2 co-crystal structures described here is applicable to other crystallographic problems where structures of several related molecules from uncharacterized single crystals are required.

Keywords: X-ray crystallography; MHC class I; HLA-A2; peptide complex; protein crystallization

Class I major histocompatibility complex (MHC‡) proteins bind peptide fragments of proteins, presenting the peptide at the cell surface. The peptide–MHC complex is recognized there by peptide-specific T-cell antigen receptors as part of a mechanism for identifying and responding to foreign antigens. Structurally, peptide presentation requires that a given peptide-binding site must accommodate any of a large number of different peptides, while exposing enough of the peptide to a T-cell receptor for specific recognition to occur. Structures of several different MHC molecules complexed with multiple endogenous peptides (Madden *et al.*, 1991, 1992; Guo *et al.*, 1992) and with single peptides (Fremont *et al.*, 1992; Silver *et al.*, 1992; Zhang *et al.*, 1992) have revealed the conformations of peptides bound to different class I MHC molecules and of two peptides differing in length bound to the murine class I molecule H-2K^b. However, a single MHC molecule is able to present a large number of different peptides of a given length, and here we address through crystallographic analysis the structural diversity in a collection of co-crystals of single peptides bound to the same MHC molecule.

We have made use of the ability to refold and crystallize single peptide–HLA-A2 complexes (Garboczi *et al.*, 1992) and of the relative ease of

† Present address: Abt. Biophysik, Max-Planck-Institut für medizinische Forschung, Postfach 10 38 20, 69028 Heidelberg, Germany.

‡ Abbreviations used: MHC, major histocompatibility complex; HLA, human leukocyte antigen; MR, molecular replacement; β_2m, β_2-microglobulin; HIV-1 RT, human immunodeficiency virus type 1 reverse transcriptase residues 309 to 317 (ILKEPVHGV); HTLV-1 Tax, human T lymphotropic virus type 1 tax protein residues 11 to 19 (LLFGYPVYV); Flu A matrix, influenza A virus matrix protein residues 58 to 66 (GILGFVFTL); HIV-1 gp120, HIV-1 gp120 residues 197 to 205 (TLTSCNTSV); Hep B, hepatitis B virus nucleocapsid residues 18 to 27 (FLPSDFFPSV); PEG, polyethylene glycol; MES, *n*-morpholinoethanesulfanolamine; $\langle I \rangle$, mean intensity; σ, standard deviation; a.u., asymmetric unit; ΔI, the difference in intensity; $\sigma\Delta I$, the standard deviation of ΔI.

0022–2836/94/240581–07 $08.00/0

structure determination by molecular replacement (MR) using the refined structure of HLA-A2 (Saper *et al.*, 1991) to determine the structures of five single peptide–HLA-A2 molecules by X-ray crystallography at −160°C. We present here the system developed to make tractable the concurrent solution of five structures. Initial data were used to determine the crystal point group *de novo*, and this information was used to guide the efficient collection of a complete dataset. Systematic absences were analyzed following data collection to permit unambiguous identification of the crystallographic space group. Three different space groups were encountered for the five co-crystals studied, and in each case, data from only a single frozen crystal were required for a complete structure determination. Successful molecular replacement solutions confirmed the space groups determined without the use of precession photography. The full structures and their interpretation are presented elsewhere (Madden *et al.*, 1993).

Preparation of peptide–HLA-A2 complexes

The HLA-A2 heavy chain and β_2-microglobulin (β_2m) were expressed as insoluble aggregates in *Escherichia coli* and renatured by dilution into refolding conditions with one of the following five viral peptides: four nonamers from human immunodeficiency virus type 1 reverse transcriptase residues 309 to 317, ILKEPVHGV, (HIV-1 RT; Tsomides *et al.*, 1991); human T lymphotropic virus type 1 tax protein residues 11 to 19, LLFGYPVYV, (HTLV-1 Tax; Utz *et al.*, 1992); influenza A virus matrix protein residues 58 to 66, GILGFVFTL, (Flu A matrix; Bednarek *et al.*, 1991; Morrison *et al.*, 1992); HIV-1 gp120 residues 197 to 205, TLTSCNTSV, (HIV-1 gp120; Garboczi *et al.*, 1992) and one decamer from hepatitis B virus nucleocapsid residues 18 to 27, FLPSDFFPSV, (Hep B; Bertoletti *et al.*, 1993). The high level of bacterial expression allows a very pure protein to be obtained upon the isolation of insoluble protein ("inclusion bodies"). To protect cysteine residues from oxidation during the isolation of the non-native proteins from bacteria, 1 to 10 mM dithiothreitol was added to all solutions. The denatured proteins were dissolved in 8 M urea and could be refolded and crystallized after up to one year of storage at −70°C. After concentration of the refolded HLA-A2 by ultrafiltration, the filtrate from the refolding solution still contains most (> 95%) of the synthetic peptide, as the peptide to heavy chain molar ratio is 10 : 1 and only 10% of the heavy chain refolds. Additional denatured heavy chain and β_2m were diluted into the filtrate to refold HLA-A2 several more times without the addition of more peptide. The five refolded peptide–HLA-A2 complexes (5 to 10 mg/ml) were stable for more than six months at 4°C.

Preparation of co-crystals

Crystallizations were performed by vapor diffusion from hanging drops in plastic 24 well plates with wells covered by plastic microscope cover slips. Equal volumes of protein (approx. 5 mg/ml) and 13 to 20% polyethylene glycol 6000 (PEG 6000), both buffered by 25 mM *n*-morpholinoethanesulfanolamine (MES) at pH 6·5 and containing 0·1% sodium azide, were mixed to form hanging drops suspended over a 13% PEG 6000 solution in 25 mM MES (pH 6·5) and 0·1% sodium azide. Crystals appeared spontaneously for the co-crystals of the Flu A matrix, HIV-1 gp120 and Hep B peptides. Hep B co-crystals grew as multiple thin plates that were improved by seeding. Microcrystals for seeding of crystal growth were prepared by crushing small or poorly formed crystals with a glass rod and serially diluting them in harvest buffer. Concentrated stock suspensions of microcrystals are very stable (> one year). Hanging drops composed of protein and varying dilutions (1 : 1, 1 : 10, 1 : 100, 1 : 1000) of microcrystals yielded observable crystal growth within 24 hours that was complete by 72 hours. Dilutions of 1 : 100 and 1 : 1000 yielded the large crystals that were used for data collection. Microseeding using homologous peptide co-crystals promoted the growth of single Hep B co-crystals to dimensions of 150 μm × 150 μm × approx. 30 μm. Microseeding with non-homologous Flu A matrix peptide co-crystals was essential for some of the crystallizations, allowing the growth of sufficiently large co-crystals of the HIV-1 RT (250 μm × 40 μm × approx. 30 μm) and the HTLV-1 Tax (500 μm × 50 μm × approx. 30 μm) peptides. Crystals showed two general morphologies: plate-like and needle-like. Except for the plate-like Hep B peptide co-crystals, the other four complexes formed crystals of both morphologies that often occurred in the same hanging drop.

Harvest and freezing of crystals

Crystals were harvested into fresh well solution containing 16% PEG 6000 (harvest buffer), except that 20% PEG 6000 was used for the HIV-1 gp120 peptide crystals. Crystals to be frozen were placed in 50 μl dialysis buttons covered with dialysis membrane and transferred in steps to harvest buffer supplemented with glycerol (20% glycerol final). Both the time at each step (1 hour to 2 days) and the size of the glycerol concentration steps (3% to 10%) were varied to determine optimal conditions, but neither gradual nor rapid changes in glycerol concentration consistently produced either higher resolution or lower mosaic spread. For freezing and mounting crystals for data collection, crystals were placed in a depression dish in a small amount of glycerol dialysis solution. The crystal was brought out of the well in a film of glycerol-supplemented harvest buffer in a loop (diameter 300 to 600 μm; Teng, 1990) of glass wool (fiber diameter 10 μm) or dental floss fiber (fiber diameter 20 μm). The loop containing the crystal was transferred to a goniometer fitted with a magnetic top so that the loop and crystal quickly entered a stream of N_2 gas cooled to −160°C by a modified Nicolet/Siemens LT-1 cryostat (Blum, 1990).

Data collection

Intensity data were collected as 0·1° oscillation images on a Xentronics multiwire area detector (Durbin *et al.*, 1986) mounted on an Elliott GX-13 rotating anode X-ray generator with a 100 μm focal cup and focusing mirrors (Harrison, 1968). The crystal-to-detector-face distance was 100 mm (120 mm for the gp120 peptide crystal). Initial data were collected from the crystals in the orientation produced by mounting. Following point-group determination, the crystal orientation was adjusted to minimize the time required for collection of a complete data set (unnecessary for triclinic crystals).

Space group determinations

The space group of each co-crystal was determined by direct analysis of the integrated diffraction intensities without the use of precession photography. Strong diffraction peaks in the first several degrees of oscillation data were identified with the BUDDHA data-reduction programs (Blum *et al.*, 1987). After conversion to reciprocal space co-ordinates using the program FRODOT (D.R.M., unpublished results), the lattice points in reciprocal space were inspected on a graphics display using the program FRODO (Jones, 1978). In this way the presence of a centered lattice and/or possible defects in the crystal (multiple lattices, etc.) could be identified. An estimate of the dimensions of the reciprocal-space unit cell was made directly from the co-ordinates of adjacent lattice points. This estimate enabled the BUDDHA autoindexing algorithm to determine the crystal orientation. Recently, the XDS data processing programs (Kabsch, 1988) have been modified to permit automatic evaluation of possible space groups on the basis of the geometry of a reduced cell determined by difference vector analysis (Kabsch, 1993). Regardless of the method used to establish the unit cell, ultimate confirmation of the space group requires analysis of the symmetry and systematic absences of the integrated diffraction intensities as described below. In addition to eliminating the need for separate precession photographs, the procedure described here determines the crystal point group early in the course of data collection, so that the time required for the acquisition of a complete data set can be minimized.

The diffraction data were integrated using the BUDDHA programs and were merged assuming triclinic crystal symmetry. The diffraction intensities were divided into batches of between 1·7° and 3·4° of contiguous oscillation data. Scale factors for each batch were calculated to equalize the mean intensity ($\langle I \rangle$) for all batches (CCP4 programs ROTAVATA/AGROVATA). The agreement between Friedel pairs indicated by the triclinic R_{sym} provided a standard for comparison in testing for the presence of other symmetry operators (Table 1).

As the unit-cell dimensions of several crystals were consistent with the presence of 2-fold symmetry axes, we compared the intensities of pairs of reflections that would be required to be equal if the symmetry operator exists. As a preliminary test, the scaled and merged "triclinic" intensities were merged again, assuming the presence of symmetry operator, so that reflections that had been distinct in the triclinic case now had the same reduced Miller indices. Without further scaling, a new R_{sym} was calculated. In several cases, the higher-symmetry R_{sym} was comparable to the R_{sym} calculated for the data as $P1$ and suggested the existence of the symmetry operator (Table 1, HIV-1 gp120 along the b-axis, Hep B along the a, b and c-axes), while in other cases (HIV-1 gp120 along the a and c-axes, HIV-1 RT along all axes) the new R_{sym} was substantially higher (usually more than twice as large) and indicated the absence of the symmetry operator under consideration. When the R_{sym} value indicated the presence of a 2-fold axis, the test was repeated for a 4-fold axis, but in no case was a 4-fold axis found, as expected from the unequal unit-cell lengths (data not shown). For comparison, the

Table 1

R_{sym} *test of 2-fold symmetry axes*

Crystal	Resol. (Å)	Unit cell: a,b,c(Å) α,β,γ(°)	R_{sym} (as $P1$)	R_{sym} (h)	R_{sym} (k)	R_{sym} (l)	Point (space) groups
HIV-1 RT	30-2·5	50·5, 63·8, 75·0 82, 76, 77	0·163	0·352	0·343	0·358	1 ($P1$)
HIV-1 gp120	30-2·6	62·6, 87·0, 79·3 90, 90, 90	0·120	0·319	0·137	0·319	2 ($P2_1$)
Hep B capsid	30-2·5	60·6, 81·1, 94·7 90, 90, 90	0·076	0·074	0·078	0·075	222 ($P2_12_12_1$)
HLA-B27†	30-2·1	45·1, 69·8, 81·1 80, 89, 90	0·156	0·346	0·485	0·482	1 ($P1$)
Flu A matrix (twin)	30-2·5	63·4, 79·2, 87·3 90, 90, 90	0·074	0·097	0·092	0·104	pseudo 222 ($P2_1$)

Overall agreement (R_{sym}) of reflections related by putative 2-fold symmetry axes along the a, b and c-axes, following data reduction by Friedel symmetry (R_{sym} for $P1$ shown for comparison). $R_{sym} = \Sigma_{hkl}(|I-\langle I \rangle|)/\Sigma_{hkl}(I)$.

† HLA-B27 (D.R.M., unpublished results).

results of the symmetry test are shown for an HLA-B27 crystal form that was clearly triclinic based on precession photography (Table 1).

It is essential for this test that the data be scaled assuming only the established symmetry (Friedel, in this case), as the imposition of a higher symmetry will cause the scaling algorithm to minimize the very differences in intensities used to test the symmetry being considered. The two-step merging process greatly increases the sensitivity of the test, so that it is possible to determine the crystal point group based on relatively incomplete data and to use this information to optimize the data collection strategy. In the first step, the data are merged assuming only established symmetries, and a "reference" R_{sym} is obtained. In the second step, the data are merged again while applying only the proposed symmetry and a new or "test" R_{sym} that reflects only the proposed symmetry is calculated. Alternatively if the data are independently merged twice while assuming point groups that differ in the proposed symmetry, the differences between reflections related by the proposed symmetry operator blend with the necessarily small differences between Friedel pairs and other genuine symmetry mates. The sensitivity of the test then depends on the ratio of the number of pairs of reflections related by the known symmetry to the number related by the putative symmetry.

We were particularly concerned about the determination of point groups for the HIV-1 gp120 peptide co-crystal, since the R_{sym} test indicated that it was monoclinic, but the β-angle of 90° implied that it might be orthorhombic. As a further test for crystallographic symmetry analogous to the spot-by-spot comparisons made in analyzing precession photographs, pairs of putatively identical intensities were compared using the program DELTAHIST. The ratio of the observed intensity difference to its standard deviation was computed for each pair, and the results for selected symmetry operators are shown as histograms in Figure 1. This test avoids the necessity for separate analysis by the precession method and compares many more pairs of spots than is usual for a small number of precession photographs. The standard deviation of the difference was computed from the standard deviations associated with each intensity measurement, and therefore required that these accurately reflect the scatter of the data. Adjustment in ROTAVATA/AGROVATA of the standard deviations determined by counting statistics was made to reflect more accurately the scatter of the data (using the parameters SDFAC and SDADD). For confirmed symmetry operators, such as the Hep B 2-fold axis along a (Figure 1B), the fraction of differences exceeding three times their standard deviation (3σ) is slightly larger (0·9%) than that expected due to random fluctuations, which presumably reflects the inaccuracy of scaling the data as triclinic. Nevertheless, the number of differences exceeding 4σ is negligible (2 of 6609), as observed for other crystallographic symmetry elements. In contrast, the presence of a substantial number of intensity differences greater than 4σ indicates the absence of the corresponding symmetry operator. This is seen for both the triclinic HIV-1 RT co-crystal (Figure 1A) and the monoclinic HIV-1 gp120 co-crystal (Figure 1C; crystallographic

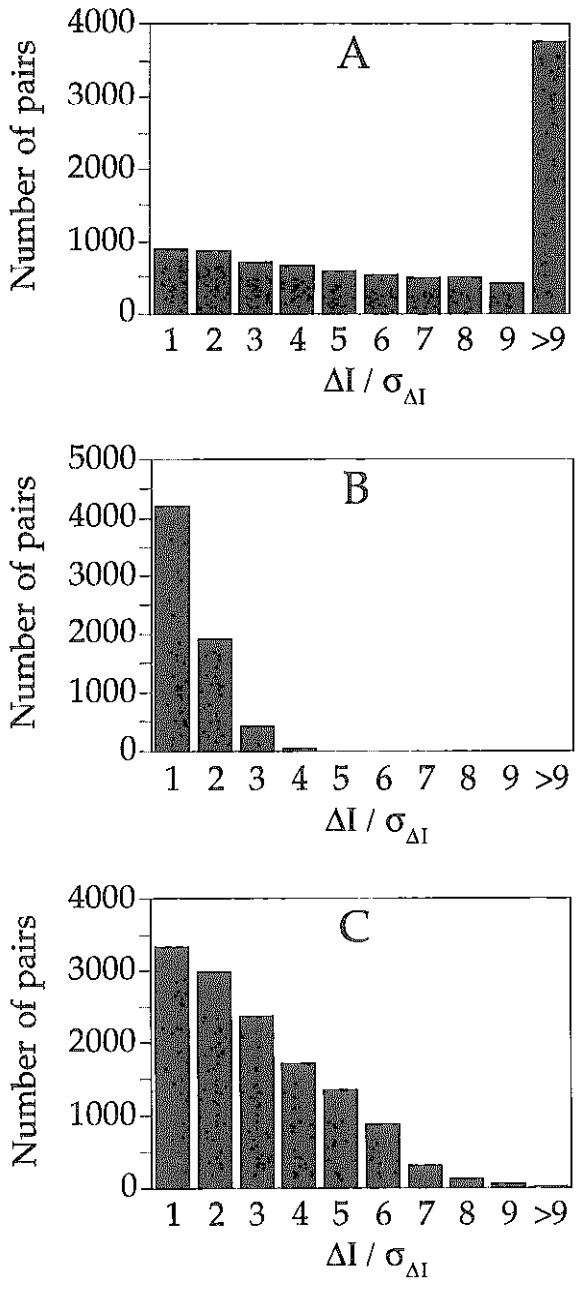

Figure 1. Testing putative 2-fold symmetry axes by pairwise comparison. The histograms show the distribution of pairs of intensities as a function of the ratio (rounded up to the nearest integer) of the intensity difference between the members of a pair (ΔI) to the standard deviation of the difference ($\sigma_{\Delta I}$). Each histogram tests whether or not there is a 2-fold axis along a. A, HIV-1 RT data, no 2-fold axis along a. B, Hep B data, 2-fold axis along a. C, HIV-1 gp120 data, pseudo-crystallographic 2-fold axis along a.

2-fold not shown). In the triclinic case (Figure 1A), the number of 8 to 9σ differences (410) is almost half the number of 0 to 1σ differences (910) and 40% of the reflections differ by more than 9σ, reflecting the lack of 2-fold symmetry. In the monoclinic crystal, the number of $>4\sigma$ differences (2734 = 21%) indicates a clear absence of crystallographic symmetry along the a-axis (Figure 1C), but the tighter clustering of the distribution around zero (compared to Figure 1A) reflects the pseudo-crystallographic nature of the non-crystallographic symmetry axis, which is almost parallel to the a-axis. This test confirmed the identification of the HIV-1 gp120 peptide co-crystal point group as monoclinic and that of the Hep B peptide co-crystal as orthorhombic.

Similar analyses (both R_{sym} and DELTAHIST) identified the Flu A matrix co-crystal as monoclinic and the HIV-1 RT and HTLV-1 Tax co-crystals as triclinic (data not shown). The point group symmetries so determined were used to calculate the final structure factor amplitudes, using the programs XDS (BUDDHA for HTLV-1 Tax co-crystal) and ROTAVATA/AGROVATA (Fox & Holmes, 1966).

For crystals exhibiting 2-fold symmetry, the presence of screw axis symmetry was tested in the complete data set by examining the intensities indexed on the reciprocal space axes that would be required to display systematic absences. An example of this analysis for the HIV-1 gp120 data is shown in Figure 2. Systematic absences are found along the b^*-axis, identifying the crystallographic 2-fold axis as a screw axis (Figure 2B) and also along the a^*-axis, reflecting the approximate 2-fold non-crystallographic screw axis (Figure 2A). This test established the HIV-1 gp120 space group as $P2_1$. The Flu A matrix co-crystal also formed in space group $P2_1$, while the Hep B co-crystal space group was found to be $P2_12_12_1$ (data not shown).

During initial characterization of the Flu A matrix peptide co-crystals, crystals with unit-cell dimensions that clearly indicated a triclinic unit cell and crystals with unit-cell dimensions very similar to the monoclinic HIV-1 gp120 co-crystal were taken from the same hanging drop. The monoclinic crystal was used to solve the Flu A matrix peptide–HLA-A2 structure, but the crushed crystals of the Flu A matrix peptide complex used as seeds were presumably a mixture of the triclinic and monoclinic space groups. One Flu A matrix peptide co-crystal was suspected of being twinned since it had unit cell dimensions of the monoclinic space group but appeared to be orthorhombic in the R_{sym} test (Table 1). A comparison of the intensity distribution of the acentric data to a Wilson distribution (Wilson, 1949) revealed relatively few weak reflections (program TRUNCATE; French & Wilson, 1978), and a tighter-than-usual clustering of the intensities around the mean intensity ($\langle I^2\rangle/\langle I\rangle^2 \approx 1{\cdot}5$, compared to 2 for a Wilson distribution; Redinbo & Yeates, 1993), both indications that the crystal was twinned. Structural work on this crystal was not pursued, but as the triclinic and monoclinic crystal forms are made up of layers of molecules containing a non-crystallographic 2-fold screw axis (see below), the twinning can be interpreted as arising from a stacking defect.

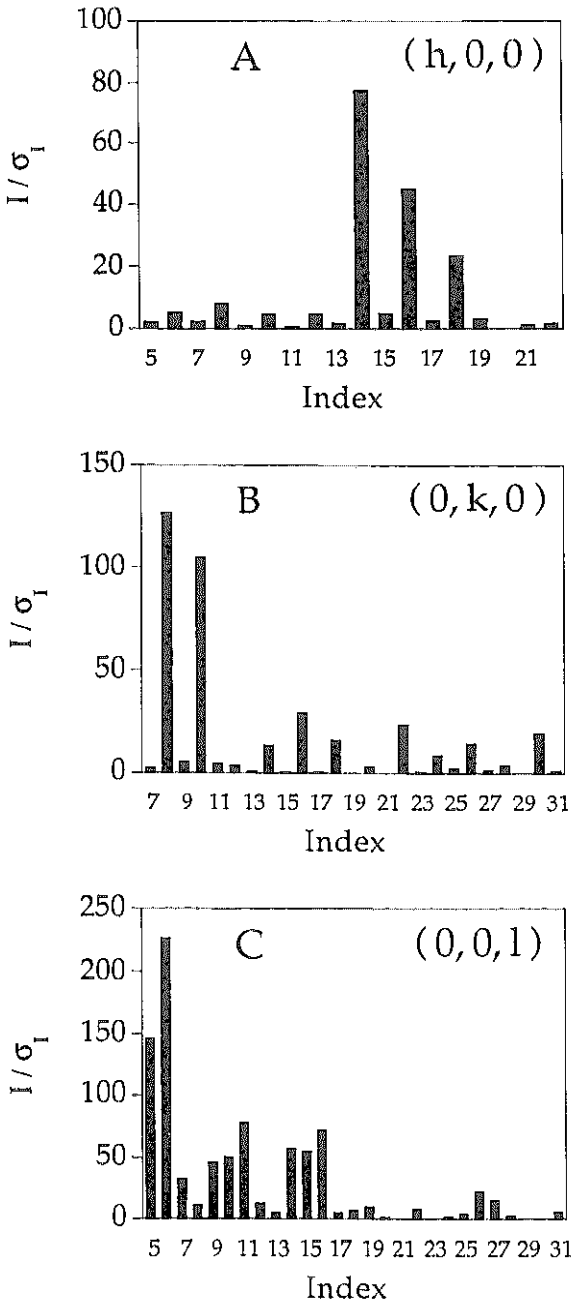

Figure 2. Test for systematic absences along the a^*, b^*, or c^*-axes for the co-crystal of the HIV-1 gp120 peptide and HLA-A2. The intensity of a reflection (I) divided by its standard deviation (σ_I) is plotted as a function of the index of the reflection along each of the reciprocal cell axes. A, (h, 0, 0): systematic absences reflect non-crystallographic 2_1 screw-axis along a; B, (0, k, 0): systematic absences reflect crystallographic 2_1 screw-axis along b; C, (0, 0, l): no systematic absences (e.g. [0, 0, 5], [0, 0, 11], [0, 0, 15]).

Molecular replacement solutions

Structure factor phases were determined by molecular replacement (program MERLOT, Fitzgerald, 1988) for one co-crystal of each space group ($P1$, HIV-1 RT; $P2_1$, HIV-1 gp120; $P2_12_12_1$, Hep B nucleocapsid) using data from 20 to 4 Å. The search model was the 2·6 Å resolution structure of HLA-A2 purified from lymphoblastoid cells and containing a mixture of peptides (Saper *et al.*, 1991).

As expected based on the comparison of calculated volumes per molecular mass unit for each of the asymmetric units (a.u.) of the three space groups (triclinic, 5·1 Å^3/Da; monoclinic, 4·9 Å^3/Da; orthorhombic, 2·6 Å^3/Da), two molecules were found in the a.u. of both the triclinic and monoclinic crystal forms. For the triclinic HIV-1 RT peptide co-crystal, a self-rotation function search yielded a clear peak, 13·9 standard deviations (σ) above the mean value, consistent with the two highest cross-rotation function peaks (11·0 and 9·9σ). A single translation function peak was found relating the two rotation function solutions (5·2σ). Following rigid-body refinement using the program X-PLOR (Brünger, 1990) of the six domains within the a.u., the $\alpha1\alpha2$, $\alpha3$ and β_2m domains for each of two molecules, R_{cryst} was 0·422 (10 to 3 Å). For the monoclinic HIV-1 gp120 peptide co-crystal, the two largest cross-rotation function peaks (6·1σ and 5·9σ) were also consistent with the top peak in a self-rotation search (4·3σ). A translation function search yielded an unambiguous placement of the two molecules (6·2σ and 7·0σ Harker section peaks for each of the rotation function solutions, and a 7·6σ peak in a 3-dimensional search between them). Following six-domain rigid-body refinement (as above), R_{cryst} was 0·398 (10 to 3 Å). As expected based on the a.u. volume, a single clear cross-rotation function peak (7·8σ) was found for the orthorhombic Hep B peptide co-crystal. The top translation function peaks on two Harker sections (7·0σ and 4·5σ) were consistent with the third largest peak on the third Harker section (3·1σ; top peak, 3·6σ). Following rigid-body refinement ($\alpha1\alpha2$, $\alpha3$ and β_2m domains), R_{cryst} was 0·415 (10 to 3 Å). Electron density maps calculated from these MR solutions, both with and without iterative real-space phase averaging (Bricogne, 1976), clearly reveal features of the structures that were not included in the starting models. These features included the bound peptides and also a five residue extension at the C terminus of the HLA-A2 heavy chain. Similarly, these features of the electron density maps were apparent for the HTLV-1 Tax and Flu A matrix co-crystals, indicating the correctness of the MR results. Since the rotation function requires correct identification of the crystal point group and since the translation function depends on the correct space group, the success of the MR calculations confirms the space group determinations for all five viral peptide–HLA-A2 co-crystals.

An examination of the molecular packing reveals that both the triclinic and monoclinic crystals are composed of stacks of two-dimensional crystals of the two-sided plane group $p12_1$. The in-plane 2-fold screw-axis forms the non-crystallographic symmetry axis in each case, while in the monoclinic crystals, the crystallographic 2-fold screw-axis runs perpendicular to the stacks, so that they form alternating layers. In the monoclinic crystals, the non-crystallographic 2-fold axis is perpendicular to the crystallographic axis, but is displaced from it by 1/10 of a unit cell; in the orthorhombic space groups $P2_12_12$ or $P2_12_12_1$ the two 2-fold axes would be required to intersect or to be displaced by 1/4 of a unit cell, respectively.

Conclusion

HLA-A2 structure determinations were performed without separate characterization of the crystal space group. As shown here, the information available early in the collection of a dataset can establish not only the lattice and unit-cell dimensions of a crystal, but also its point group, which is sufficient to determine the most efficient strategy for completing data collection, frequently avoiding the need to collect an entire triclinic hemisphere of data. Translational components of the crystal symmetry can be identified by inspection of systematic absences in the complete data set, establishing the crystal space group (with a possible ambiguity in the handedness of some screw axes). In practice, therefore, a single crystal can suffice for a complete MR structure determination, even when the space group of the new crystal is unknown in advance. This system is particularly useful for structural work on a series of site-directed mutants or ligand complexes where crystals are found to form in multiple space groups. In addition, the symmetry determination strategy can also be applied to structure determinations when the breakdown of an apparent crystallographic symmetry operator is suspected at higher resolution.

The authors thank U. Utz and W. Biddison for helpful discussions and the gift of the HTLV-1 Tax peptide, Professor Jack Strominger for his initial and continuing collaboration, Scott Garman for advice on crystal twinning, and other members of our laboratory for discussions and support. This work was supported by the National Institutes of Health (D.N.G., D.R.M.) and the Howard Hughes Medical Institute (D.C.W.).

References

Bednarek, M. A., Sauma, S. Y., Gammon, M. C., Porter, G., Tamhankar, S., Williamson, A. R. & Zweerink, H. J. (1991). The minimum peptide epitope from the influenza virus matrix protein. *J. Immunol.* **147**, 4047–4053.

Bertoletti, A., Chisari, F. V., Penna, A., Guilhot, S., Galati, L., Missale, G., Fowler, P., Schlicht, H.-J., Vitiello, A., Chesnut, R. C., Fiaccadori, F. & Ferrari, C. (1993). Definition of a minimal optimal cytotoxic T-cell epitope within the hepatitis B virus nucleocapsid protein. *J. Virol.* **67**, 2376–2380.

Blum, M. (1990). The structure of a VSG variable domain from *Trypanosoma brucei* at 2·7 Å resolution. Ph.D. thesis, Harvard University.

Blum, M., Metcalf, P., Harrison, S. C. & Wiley, D. C. (1987). A system for collection and on-line integration of X-ray diffraction data from a multiwire area detector. *J. Appl. Crystallogr.* **20**, 235–242.

Bricogne, G. (1976). Methods and programs for direct-space exploitation of geometric redundancies. *Acta Crystallogr. sect. A*, **32**, 832–847.

Brünger, A. (1990). X-PLOR (Version 2.1) Manual. Yale University, New Haven, Connecticut.

Durbin, R., Burns, R., Moulai, J., Metcalf, P., Freymann, D., Blum, M., Anderson, J., Harrison, S. C. & Wiley, D. C. (1986). Protein, DNA, and virus crystallography with a focused imaging proportional counter. *Science*, **232**, 1127–1132.

Fitzgerald, P. M. D. (1988). MERLOT, an integrated package of computer programs for the determination of crystal structures by molecular replacement. *J. Appl. Crystallogr.* **21**, 273–278.

Fox, G. C. & Holmes, K. C. (1966). An alternative method of solving the layer scaling equations of Hamilton, Rollett, and Sparks. *Acta Crystallogr.* **20**, 886–891.

Fremont, D. H., Matsumura, M., Stura, E. A., Peterson, P. A. & Wilson, I. A. (1992). Crystal structures of two viral peptides in complex with murine MHC class I H-2K^b. *Science*, **257**, 919–927.

French, S. & Wilson, K. (1978). On the treatment of negative intensity observations. *Acta Crystallogr. sect. A*, **34**, 517–525.

Garboczi, D. N., Hung, D. T & Wiley, D. C. (1992). HLA-A2-peptide complexes: refolding and crystallization of molecules expressed in *Escherichia coli* and complexed with single antigenic peptides. *Proc. Nat. Acad. Sci., U.S.A.* **89**, 3429–3433.

Guo, H.-C., Jardetzky, T. S., Garrett, T. P. J., Lane, W. S., Strominger, J. L. & Wiley, D. C. (1992). Different length peptides bind to HLA-Aw68 similarly at their ends but bulge out in the middle. *Nature (London)*, **360**, 364–366.

Harrison, S. C. (1968). A point-focusing camera for single-crystal diffraction. *J. Appl. Crystallogr.* **1**, 84–90.

Jones, T. A. (1978). A graphics model building and refinement system for macromolecules. *J. Appl. Crystallogr.* **11**, 268–272.

Kabsch, W. (1988). Evaluation of single crystal X-ray diffraction data from a position-sensitive detector. *J. Appl. Crystallogr.* **21**, 916–924.

Kabsch, W. (1993). Automatic processing of rotation diffraction data from crystals of initially unknown symmetry and cell constants. *J. Appl. Crystallogr.* **26**, 795–800.

Madden, D. R., Gorga, J. C., Strominger, J. L. & Wiley, D. C. (1991). The structure of HLA-B27 reveals nonamer self-peptides bound in an extended conformation. *Nature (London)*, **353**, 321–325.

Madden, D. R., Gorga, J. C., Strominger, J. L. & Wiley, D. C. (1992). The three-dimensional structure of HLA-B27 at 2·1 Å resolution suggests a general mechanism for tight peptide binding to MHC. *Cell*, **70**, 1035–1048.

Madden, D. R., Garboczi, D. N. & Wiley, D. C. (1993). The antigenic identity of peptide/MHC complexes: a comparison of the conformations of five viral peptides presented by HLA-A2. *Cell*, **75**, 693–708.

Morrison, J., Elvin, J., Latron, F., Gotch, F., Moots, R., Strominger, J. L. & McMichael, A. (1992). Identification of the nonamer peptide from influenza: a matrix protein and the role of pockets of HLA-A2 in its recognition by cytotoxic T lymphocytes. *Eur. J. Immunol.* **22**, 903–907.

Redinbo, M. R. & Yeates, T. O. (1993). Structure determination of plastocyanin from a specimen with a hemihedral twinning fraction of one-half. *Acta Crystallogr. sect. D*, **49**, 375–380.

Saper, M. A., Bjorkman, P. J. & Wiley, D. C. (1991). Refined structure of the human histocompatibility antigen HLA-A2 at 2·6 Å resolution. *J. Mol. Biol.* **219**, 277–319.

Silver, M. L., Guo, H.-C., Strominger, J. L. & Wiley, D. C. (1992). Atomic structure of a human MHC molecule presenting an influenza virus peptide. *Nature (London)*, **360**, 367–369.

Teng, T.-Y. (1990). Mounting of crystals for macromolecular crystallography in a free-standing thin film. *J. Appl. Crystallogr.* **23**, 387–391.

Tsomides, T. J., Walker, B. D. & Eisen, H. N. (1991). An optimal viral peptide recognized by CD8$^+$ T cells binds very tightly to the restricting class I major histocompatibility complex protein on intact cells but not to the purified class I protein. *Proc. Nat. Acad. Sci., U.S.A.* **88**, 11276–11280.

Utz, U., Koenig, S., Coligan, J. E. & Biddison, W. E. (1992). Presentation of 3 different viral peptides, HTLV-1 Tax, HCMV gB, and influenza virus M1 is determined by common structural features of the HLA-A2. 1 molecule. *J. Immunol.* **149**, 214–221.

Wilson, A. J. C. (1949). The probability distribution of X-ray intensities. *Acta Crystallogr.* **2**, 318–321.

Zhang, W., Young, A. C. M., Imarai, M., Nathenson, S. G. & Sacchettini, J. C. (1992). Crystal structure of the major histocompatibility complex class I H-2K^b molecule containing a single viral peptide: implications for peptide binding and T-cell receptor recognition. *Proc. Nat. Acad. Sci., U.S.A.* **89**, 8403–8407.

Edited by A. Klug

(Received 20 December 1993; accepted 10 March 1994)